ACS APPLIED MATERIALS & INTERFACES

Research Article

www.acsami.org

High-Rate $LiTi_2(PO_4)_3$@N–C Composite via Bi-nitrogen Sources Doping

Dan Sun,[†] Xia Xue,[†] Yougen Tang,[†] Yan Jing,[‡] Bin Huang,[§] Yu Ren,[∥] Yan Yao,[‡] Haiyan Wang,[*,†,⊥] and Guozhong Cao[*,§]

[†]College of Chemistry and Chemical Engineering, Central South University, Changsha, 410083, People's Republic of China

[‡]Department of Electrical and Computer Engineering, University of Houston, Houston, Texas 77204, United States

[§]Department of Materials Science & Engineering, University of Washington, Seattle, Washington 98185, United States

[∥]Battery Materials, BASF (China) Co., Ltd., Shanghai, 201206, People's Republic of China

[⊥]State Key Laboratory for Powder Metallurgy, Central South University, Changsha 410083, People's Republic China

Supporting Information

ABSTRACT: Mesoporous $LiTi_2(PO_4)_3$@nitrogen-rich doped carbon composites have been synthesized by a novel bi-nitrogen sources doping strategy. Tripolycyanamide ($C_3H_6N_6$) and urea are proposed for the first time as both nitrogen and carbon sources to achieve a homogeneous nitrogen-doped carbon coating layer via an in situ method. The electrode delivers ultrahigh rate performance and outstanding cycling stability in lithium ion batteries (LIBs). In an organic electrolyte system, the electrode demonstrates high discharge capacities of 120 mAh g^{-1} and 87 mAh g^{-1} at 20C and 50C, respectively. Moreover, 89.5% of initial discharge capacity is retained after 1000 cycles at 10C. When used as an anode for aqueous LIBs, the electrode also demonstrates superior rate capability with the discharge capacity of 103 mAh g^{-1} at 10C, corresponding to 84% of that at 1C. Outstanding cycling stability with capacity retention of 91.2% after 100 cycles at 30 mA g^{-1} and 90.4% over 400 cycles at 150 mA g^{-1} are also demonstrated. The uniform nitrogen-rich carbon coating and unique mesoporous structure play important roles in effectively suppressing the charge-transfer resistance and facilitating Li ion/electron diffusion, thus leading to the superior electrochemical properties.

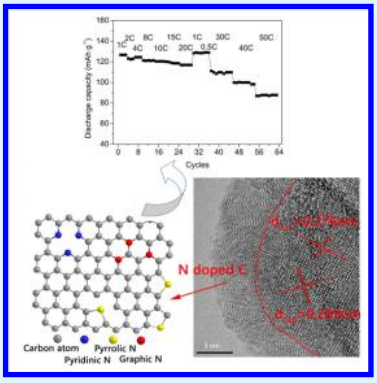

KEYWORDS: *aqueous lithium ion battery, nitrogen doping, mesoporous $LiTi_2(PO_4)_3$/C, rate performance, cycling performance*

INTRODUCTION

During the past decades, LIBs have dominated the portable electronic markets, and they exhibit huge potential for electric vehicles (EVs) and large-scale energy storage systems (ESSs) in the near future.[1] However, the concerns for safety and high cost due to the employment of combustible organic electrolytes greatly narrow their extensive applications. Aqueous lithium ion batteries (ALIBs), which use cheap inorganic salt solution as electrolyte, could fundamentally eliminate the safety issue and rigorous assembly conditions at the same time.[2] Other advantages, such as higher ionic conductivity of electrolyte, more environmental benignity, and lower cost could also be achieved for ALIBs.[2]

Because of the narrow electrochemically stable window of electrolyte, the available electrode materials, especially the anode materials, are seriously confined. Generally, the traditional cathode materials in LIBs like $LiFePO_4$,[3] $LiNi_{1/3}Co_{1/3}Mn_{1/3}O_2$,[4] $LiCoO_2$,[5] and $LiMn_2O_4$[6] have been well investigated as the cathodes for ALIBs. However, the anodes for ALIBs are restricted to the electrode materials with Li ion operation potential of 2–3 V versus Li^+/Li,[7] there are only a few suitable candidates, for example, vanadates and $LiTi_2(PO_4)_3$. The first ALIB of $VO_2//LiMn_2O_4$ was constructed by Dahn et al., cycling for limited cycles.[8] Since then, the ALIB systems, such as $LiV_3O_8//LiMn_2O_4$, $NaV_3O_8//LiMn_2O_4$, $LiV_3O_8//LiNi_{0.81}Co_{0.19}O_2$, $NaV_6O_{15}//LiMn_2O_4$, and so on, have been proposed based on vanadates anodes.[5,9−11] Unfortunately, most vanadates demonstrated poor cycling stability which may originate from the degradation of crystal structure and vanadium dissolution in aqueous solution.[7] $LiTi_2(PO_4)_3$/C is believed to be a promising anode material for ALIB by virtues of its good cycling durability and relatively low working potential. Xia's group reported a piece of milestone work in ALIBs by eliminating the soluble oxygen in Li_2SO_4 solution. The cycling life of as-constructed $LiTi_2(PO_4)_3//LiFePO_4$ ALIB at relatively high current rate (6C-rate) was significantly improved.[12] Even so, the performance of ALIBs system, particularly at low current densities, is still far from practical applications.

$LiMn_2O_4$ has been proved to be a promising cathode for ALIBs benefiting from its low cost, high voltage potential and remarkable cycling stability in aqueous solution.[5] In contrast,

Received: September 15, 2015
Accepted: December 3, 2015
Published: December 3, 2015

DOI: 10.1021/acsami.5b08697
ACS Appl. Mater. Interfaces 2015, 7, 28337–28345

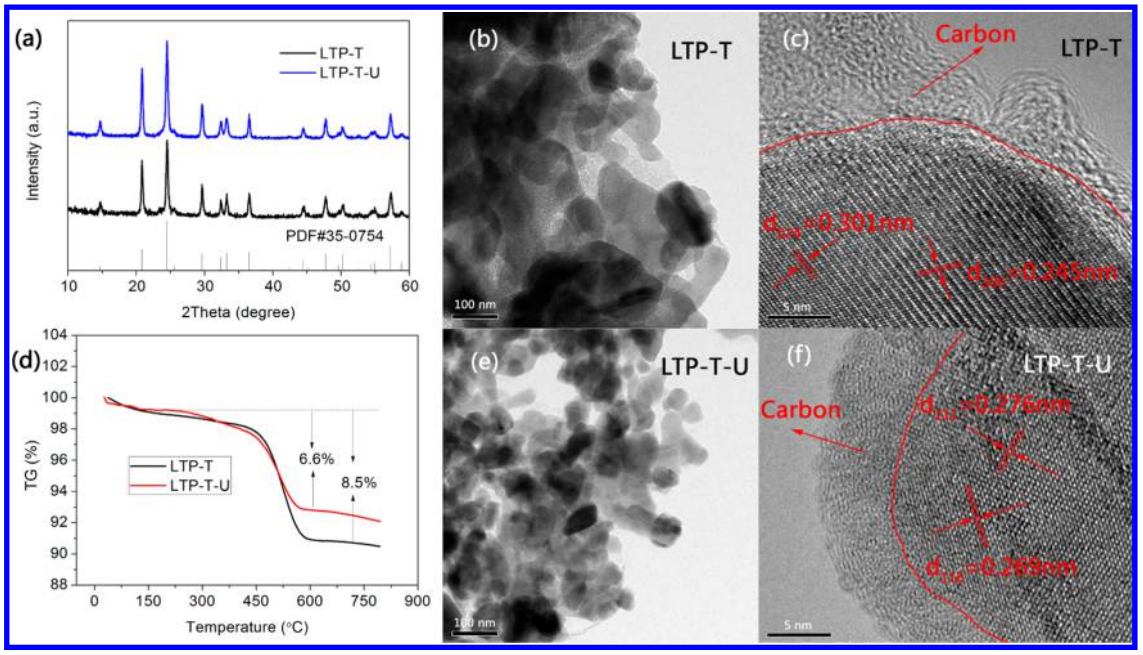

Figure 1. (a) XRD patterns of LTP-T and LTP-T-U; (b) TEM and (c) HRTEM images of LTP-T; (d) TGA curves of LTP-T and LTP-T-U; (e) TEM, (f) HRTEM images of LTP-T-U.

the electrochemical properties of as-reported anodes for ALIBs are much insufficient. Electrochemical properties of pristine $LiTi_2(PO_4)_3$ are seriously restricted by its low electronic conductivity,[13] which could be well overcome by size reducing and carbon coating.[14] It is well-known that high-quality carbon coating can not only largely improve the electronic conductivity of materials but also protect inner material from electrolyte flushing, generating better electrochemical performance.[15,16] In our previous work, $LiTi_2(PO_4)_3$ nanoparticles coated with high-quality carbon were prepared, which demonstrated outstanding cycling stability over 300 cycles at 0.2C.[17] Unfortunately, its rate capability was not very good. Recently, intensive researches have revealed that the electronic conductivity of carbon layers could be improved by surface modification (such as doped with N, B, and O), thanks to the enhanced electron properties, pseudocapacitance effect and extra Li^+ storage sites after surface atomic modification.[18,19] The N-modified composites with significantly enhanced electrochemical properties, such as N-doped graphene,[18−20] N-doped g-C_3N_4/MoS_2,[21] N-doped graphene/SnO_2,[22] N-doped nanoporous carbon,[23] N-doped Sn/C,[24] N-doped rGO/Sn,[25] N-doped CNT/$LiFePO_4$,[26] and N-doped Fe_3O_4/C[27] have been reported. As far as we know, the nitrogen modified $LiTi_2(PO_4)_3$/C has not been reported yet. In addition, mesoporous materials are attracting more and more attention by virtue of the large contact surface area between electrode and electrolyte allowing both Li^+ and electron to migrate rapidly, thus resulting in superior rate performance.[28−31]

Herein, a novel bi-nitrogen sources doping approach is proposed to fabricate mesoporous and nitrogen-rich doped $LiTi_2(PO_4)_3$@C composite. This strategy is completely different from conventional nitrogen doping methods, in which the NH_3 gas or amine was used as a single nitrogen source.[23,32,33] In our work, tripolycyanamide ($C_3H_6N_6$) is proposed for the first time as both carbon and nitrogen source to achieve homogeneous nitrogen doped carbon coating layer via an in situ method. Moreover, urea ($CO(NH_2)_2$) is also introduced to improve the content of nitrogen in carbon layer and generate massive nanopores at the same time. Accordingly, the nitrogen content in carbon is as high as 11.1%. This strategy possesses characteristics of low cost, available and also permits facile scale-up for mass production. Benefiting from high nitrogen doping content and the unique structure, the as-prepared electrode demonstrates ultrahigh rate capability and outstanding cycling life.

RESULTS AND DISCUSSION

The XRD patterns of as-obtained LTP-T and LTP-T-U composites are presented in Figure 1a. The two samples demonstrate the same diffraction peaks, which are in great agreement with the rhombohedral NASICON type $LiTi_2(PO_4)_3$ phase (JCPDS #35-0754) with a *R*3*c* space group. The absence of impurity peaks reflects the high purity of $LiTi_2(PO_4)_3$ phase in the samples. The calculated lattice parameters (Table S1) of LTP-T and LTP-T-U match well with previous reports.[34,35]

The microstructural features of as-prepared composites are displayed in Figure 1. From the TEM picture of LTP-T (Figure 1b), the LTP-T is of individual particles with size range of 50−70 nm. The HRTEM image of LTP-T (Figure 1c) clearly shows that the surface of the $LiTi_2(PO_4)_3$ particle was coated with an amorphous carbon layer. As deduced from the image, the interplanar spacing is 0.301 and 0.245 nm, corresponding to the *d*-spacing of the (024) and (300) crystal face of rhombohedral $LiTi_2(PO_4)_3$, respectively. The N_2 adsorption−desorption isotherm of LTP-T is shown in Figure S1a, in which there is a typical IV isotherm, suggesting the existence of mesoporous structure. Brunauer−Emmett−Teller (BET) surface area of LTP-T is 75.9 m^2 g^{-1}. Figure 1e gives the TEM image of LTP-T-U, as displayed, the particle size decreases to 30−50 nm. Moreover, better particle dispersion and more obvious pores are observed in comparison with LTP-T. The HRTEM image of LTP-T-U (Figure 1f) displays uniform carbon layer whose thickness is ∼5 nm. As reported, the thickness of carbon layer around 4−8 nm on electrode

DOI: 10.1021/acsami.5b08697
ACS Appl. Mater. Interfaces 2015, 7, 28337−28345

materials could reach a good balance of Li^+ diffusion and electron conductivity, promising superior electrochemical properties.[15] Obviously, it is the in situ coating strategy that creates the uniform carbon layer. In this method, the carbon source could be well coated on the surface of precursor when separating from glycol. The interplanar spacing of 0.269 and 0.276 nm deduced from the HRTEM picture (Figure 1f) corresponds well to the *d*-spacing of the (116) and (211) plane of rhombohedral $LiTi_2(PO_4)_3$.

The BET surface area of LTP-T-U is 87.6 $m^2 \cdot g^{-1}$ (Figure S1b), larger than that of LTP-T. Meanwhile, LTP-T-U also displays amounts of pores with larger size arrange of 5−8 nm and 30−40 nm (Figure 2b) than that of LTP-T (Figure 2a).

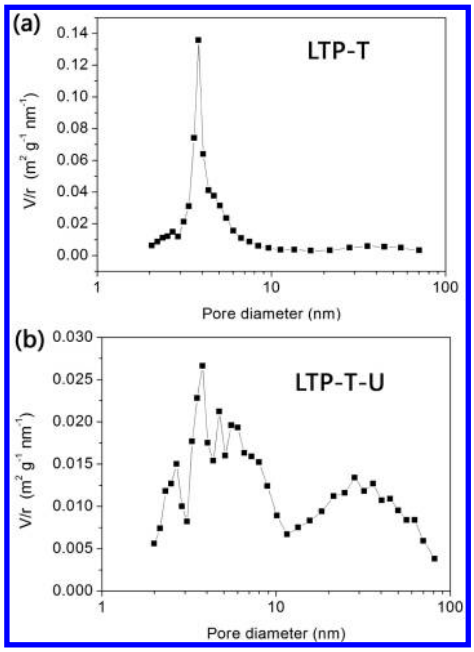

Figure 2. Barrett−Joyner−Halenda (BJH) pore size distribution plot of (a) LTP-T and (b) LTP-T-U.

Obviously, the increase of pore size originates from the addition of urea, which has been widely used as pore-forming agent.[36] As we know, the pore size significantly affects the rate performance of nanoporous materials.[28] Generally, the larger pores could enable ions to diffuse into the crystal from the electrolyte more easily, leading to better rate performance.[37] The carbon contents of LTP-T and LTP-T-U composites are measured by TGA. As recorded in Figure 1e, the amount of coated carbon of LTP-T-U is 6.6 wt %, which is less than that of LTP-T (8.5 wt %). The optimum carbon coating could further increase the electronic conductivity of electrode material without sacrificing tap density and energy density.

X-ray photoelectron spectroscopy (XPS) is applied for the surface element analysis of as-prepared samples. Elements of Ti, C, O, P, and N can be observed in the survey spectrum of both LTP-T (Figure 2a) and LTP-T-U (Figure 2b). Note that the atomic ratio of N/C is 5.4 and 11.1% for LTP-T and LTP-T-U according to the peak area ratio of N 1s to C 1s, respectively. Apparently, the increase of nitrogen content is resulted from the addition of urea. The N/C ratio in LTP-T-U here is higher than those in ref 20 (∼3.9%), ref 38 (∼8.9%), ref 39 (∼5.6%), and ref 40 (∼10.1%). Apparently, a high quality carbon layer with more nitrogen doping could be achieved via our bi-nitrogen sources doping approach. Although the influence of nitrogen doping to the conductivity of carbon has not been well illustrated, the relatively high content is always expected to be favorable.[40] The high-resolution XPS spectra of O, P, and Ti of LTP-T and LTP-T-U (Figure S2) are similar and match well the reported $LiTi_2(PO_4)_3$.[41] The high-resolution N 1s XPS spectra of two samples (Figure 3b) can be deconvoluted into four different signals. The peak at ∼402.2 eV corresponds to the N in N−O bond.[42] The peaks at ∼400.6, ∼ 399.3, and ∼398.2 eV, are attributed to graphitic N, pyrrolic N, and pyridinic N, respectively, as explained in Figure 3d.[19] Note that the graphic N is dominant in the LTP-T product. While the intensity of graphic N in LTP-T-U decreases clearly in comparison with LTP-T. Theoretical calculations imply that pyrrolic N and pyridinic N doping are more beneficial than graphic N for Li storage.[43] The high-resolution spectrum of C

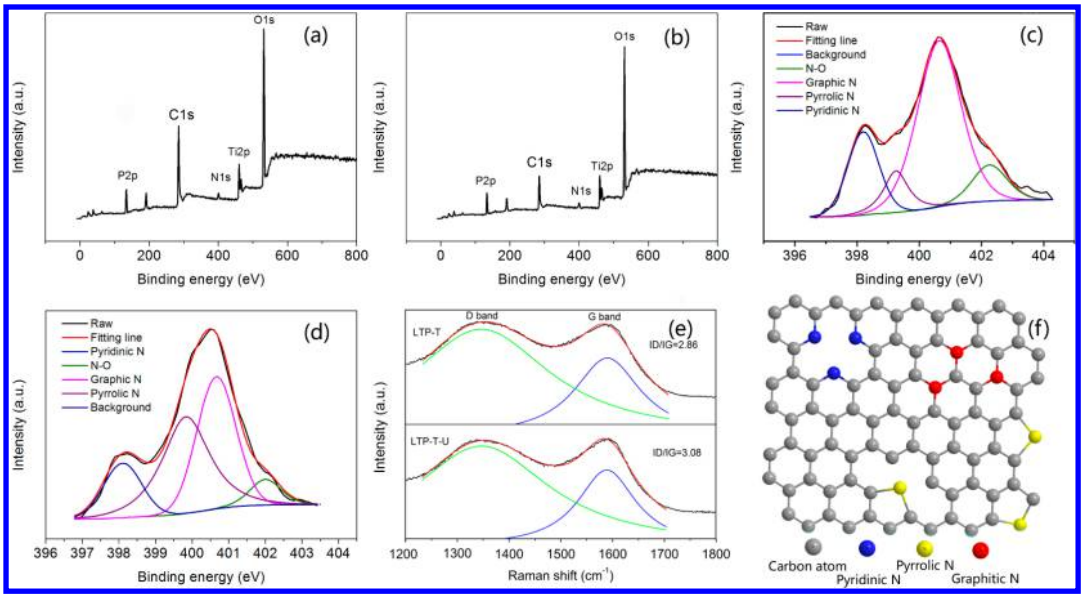

Figure 3. Survey XPS spectra of (a) LTP-T and (b) LTP/C-T-U; high-resolution XPS spectra of (c) LTP-T and (d) LTP/C-T-U; (e) Raman spectra of LTP-T and LTP/C-T-U; and (f) illustration of nitrogen doping carbon with different doping sites.

DOI: 10.1021/acsami.5b08697
ACS Appl. Mater. Interfaces 2015, 7, 28337−28345

1s in LTP-T-U could be fitted by several peaks corresponding to O−C═O, (289.2 eV), C═O (288.0 eV), C−O (286.7 eV), C−N (285.6 eV), and C−C (284.6 eV) further suggests the presence of C−N (Figure S2).[17] The XPS results also reveal that the N atoms are mainly doped in carbon layers instead of $LiTi_2(PO_4)_3$. To know more about the structure of the carbon layer, Raman spectroscopy was performed (Figure 3c). The two strong bands around 1600 and 1330 cm^{-1} could be ascribed to the in-plane vibrations of crystalline graphitic carbon (G band) and disordered amorphous carbon (D band), respectively. The relatively high I_D/I_G value for LTP-T-U (3.08) indicates a more disordered feature in comparison with that of LTP-T (2.86), which may relate to the defects in carbon because of the more N atoms doping.[19] It is well-known that the homogeneity of nitrogen doping and carbon coating significantly affect the properties of electrode.[44] Therefore, the scanning transmission electron microscope-energy dispersive spectrometer (STEM-EDS) elemental mapping was performed. As seen in Figure 4,

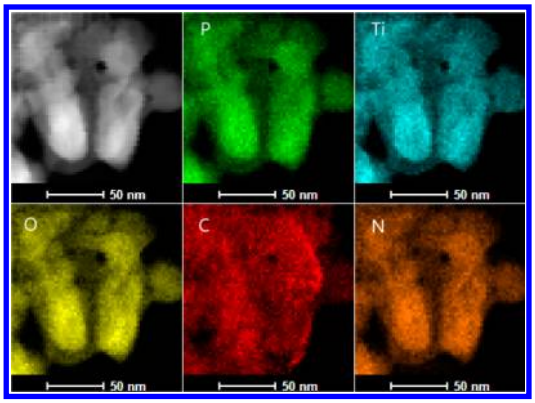

Figure 4. STEM-EDS images of LTP-T-U.

the appearance of Ti, P, O, C, and N atoms are almost the same, implying the uniformly nitrogen doping and carbon coating. In summary, a homogeneous and nitrogen-rich carbon layer has been successfully achieved.

Electrochemical Properties in Nonaqueous LIBs. First, we performed the electrochemical test of as-prepared samples in organic electrolyte cells. The rate performance of LTP-T-U and LTP-T is compared in Figure 5a. LTP-T delivers a discharge capacity of 131 mAh g^{-1} at 1C and 89 mAh g^{-1} at 20C, respectively. While LTP-T-U exhibits much better rate performance with a discharge capacity of 128 mAh g^{-1} at 1C and 120 mAh g^{-1} at 20C, respectively. When the charge/discharge rate is increased to 40C and 50C, LTP-T-U still delivers 101 and 87 mAh g^{-1}, respectively. In other words, 1.5 min charge can retain a high capacity of 101 mAh g^{-1}. Note that when the current density returns to low value (1C) after high rate test, the capacity could be fully recovered to the original value, revealing that the electrode could be tolerant to ultrafast charge/discharge process. To our best knowledge, no literature has reported such high rate capability for $LiTi_2(PO_4)_3$/C electrode over 10C. So far the best result for $LiTi_2(PO_4)_3$/C electrode in organic electrolyte is 103 mAh g^{-1} at 10C rate,[34] while our material demonstrates the same capacity under 3 times higher current density (40C). Moreover, although the theoretical capacity of $LiTi_2(PO_4)_3$ is relatively low (138 mAh g^{-1}), the discharge capacity of LTP-T-U at extremely high current density here is higher than those of graphene-modified $LiFePO_4$ (~86 mAh g^{-1} at 30C),[45] N-CNTs modified $LiFePO_4$ (~50 mA g^{-1} at 10C),[26] TiN modified $Li_4Ti_5O_{12}$ (~70 mAh g^{-1} at 20C),[46] $LiMn_2O_4$ porous nanorods (~83 mAh g^{-1} at 30 C),[47] $Na_{1.08}V_3O_8$ nanosheets (~72.6 mAh g^{-1} at 50C).[48] Figure 5b displays the charge/discharge curves of LTP-T-U at various rates. There are a short platform at ~2.75 V (vs Li^+/Li) and a long voltage platform at ~2.45 V (vs Li^+/Li) at 0.5C. When raising the current rate, flat platforms are well maintained despite of the increase of overpotential. Moreover, remarkable durability at extremely high current density was observed for LTP-T-U. As demonstrated in Figure 5c, LTP-T-U delivers an initial capacity

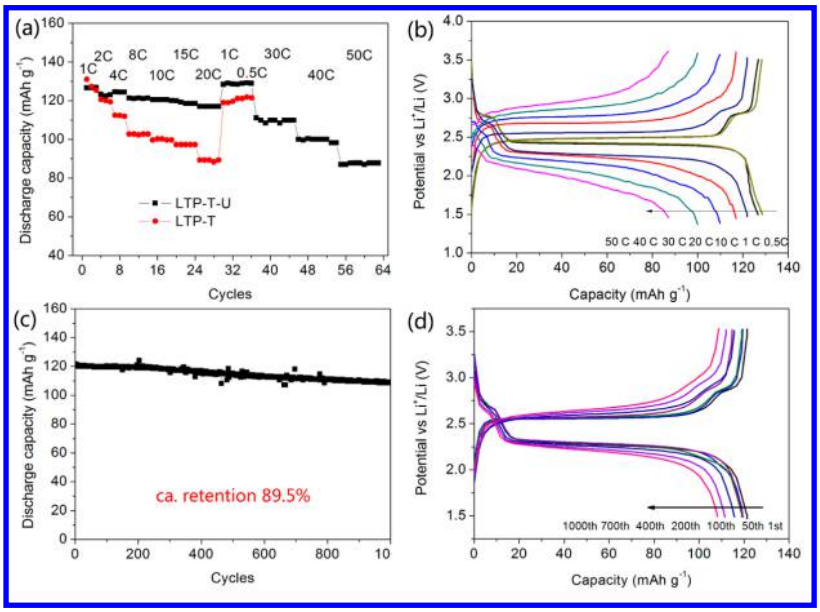

Figure 5. (a) The discharge capability of LTP-T and LTP-T-U at different rates (1C = 150 mA g^{-1}); (b) the charge/discharge curves of LTP-T-U at different rates; (c) the cycling stability of LTP-T-U at 10C; (d) the charge/discharge curves of LTP-T-U after different cycles at 10C. The capacity is calculated based on the mass of $LiTi_2(PO_4)_3$.

DOI: 10.1021/acsami.5b08697
ACS Appl. Mater. Interfaces 2015, 7, 28337−28345

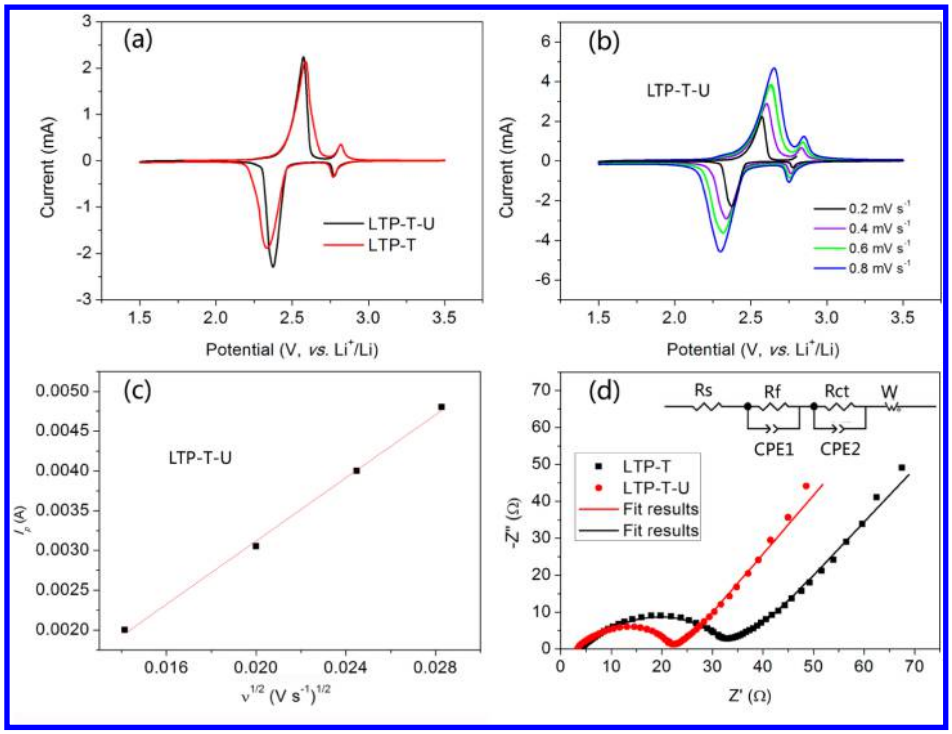

Figure 6. (a) CV curves of LTP-T and LTP-T-U; (b) the CV curves of LTP-T-U at various sweep rates; (c) the relationship between the peak current (I_p) and the square root of scan rate ($\nu^{1/2}$) of LTP-T-U; (d) the Nyquist plots of LTP-T and LTP-T-U and (inset) the equivalent circuit model.

of 122 mAh g^{-1} at 10C and a capacity retention of 89.5% after 1000 cycle. This implies that the $LiTi_2(PO_4)_3$@C electrode here could tolerate rapidly charge/discharge test without obvious structure degradation after long cycles, which is a desirable characteristic for high power applications. Figure 5d presents the charge/discharge curves of LTP-T-U after different cycles. On the cycles increasing, the voltage platform remains well, though the main platform shrinks and polarization increases slightly, which might be related to the slight capacity fading.

Figure 6a shows the CV curves of LTP-T and LTP-T-U at a scanning rate of 0.2 mV s^{-1}, in which similar redox peaks at 2.3/2.6 V and 2.8/2.9 V are demonstrated, respectively. While the polarization potential of the LTP-T-U is lower than that of LTP-T. Additionally, LTP-T-U has narrower half peak width. These facts indicate better charge transfer kinetics of LTP-T-U and correspond well with its better rate performance. Figure 6b displays the CV curves of LTP-T-U at different sweep rates. As seen, the polarization potential increases with the increasing of sweep rate. At the high scan rate of 0.8 mV s^{-1}, the sharp redox peaks are still maintained. The ratio of anodic peak current to cathodic peak current (I_{pa}/I_{pc}) is a significant indicator to reveal the reversibility of the Li^+ insertion/extraction reaction. For a Nernstian wave with a stable product, $I_{pa}I_{pc}$ should be equal to unity, and the electrode reversibility is better when the I_{pa}/I_{pc} is close to unity.[46] Table S2 lists the I_{pa}/I_{pc} values of the sample LTP-T-U at different sweep curves. The small values confirm its good Li^+ diffusion kinetics.[46] The relationship between the I_p and the $\nu^{1/2}$ for LTP-T-U is demonstrated in Figure 6c. As seen, the I_p vs $\nu^{1/2}$ for the sample approaches to a straight line, indicating the semidiffusion controlled process of the Li^+ insertion into the sample, which could be regarded as a quasi-reversible system.[46,49]

To further evaluate the electrochemical interfacial properties, we performed EIS tests of LTP-T-U and LTP-T. The Nyquist plots (Figure 6d) of activated LTP-T and LTP-T-U electrodes after 5 cycles demonstrate two depressed semicircles and a slope line. Generally, the small intercept represents the solution impedance of the cells (R_s). The first semicircle in the high frequency (R_f) relates to the interface parameters like porous mature of electrode, the bulk of materials, or surface film contribution, and the semicircle in the mediate frequency is due to the charge-transfer resistance (R_{ct}).[50,51] The slope line at low frequency reflects the Warburg impedance (Z_w), implying the Li^+ transfer in the solid electrode. Clearly, the R_f and R_{ct} of the LTP-T-U electrode are smaller than those of the LTP-T (Table S3). The suppressed impedance is clearly related to the richer mesoporous structure that facilitates the Li^+ diffusion between electrode and electrolyte. Meanwhile, the remarkably improved electronic conductivity by the uniform nitrogen-rich carbon layer also contributes to the decrease of impedance. The four-point probe test results demonstrate that the electronic conductivity of LTP-T-U (2.86×10^{-2} S cm^{-1}) is closed to eight times higher than that of LTP-T (3.29×10^{-3} S cm^{-1}). Apparently, the superior electrochemical properties of LTP-T-U are mainly attributed to the homogeneous nitrogen-rich carbon coating as well as the unique mesoporous structure.

Electrochemical Properties in ALIB. Considering the superior electrochemical properties of LTP-T-U in organic electrolyte, the electrochemical behavior in aqueous electrolyte is also investigated. At first, a three-electrode CV method was employed to investigate the Li ion insertion/extraction behaviors of individual LTP-T-U and $LiMn_2O_4$, respectively. As displayed in Figure S3, LTP-T-U shows two redox couples at −0.84/−0.72 V and −0.43/−0.42 V versus SCE. Good lithium insertion/extraction behaviors with two redox couples at 0.80/0.78 V and 0.92/0.90 V vs SCE were also observed for

DOI: 10.1021/acsami.5b08697
ACS Appl. Mater. Interfaces 2015, 7, 28337−28345

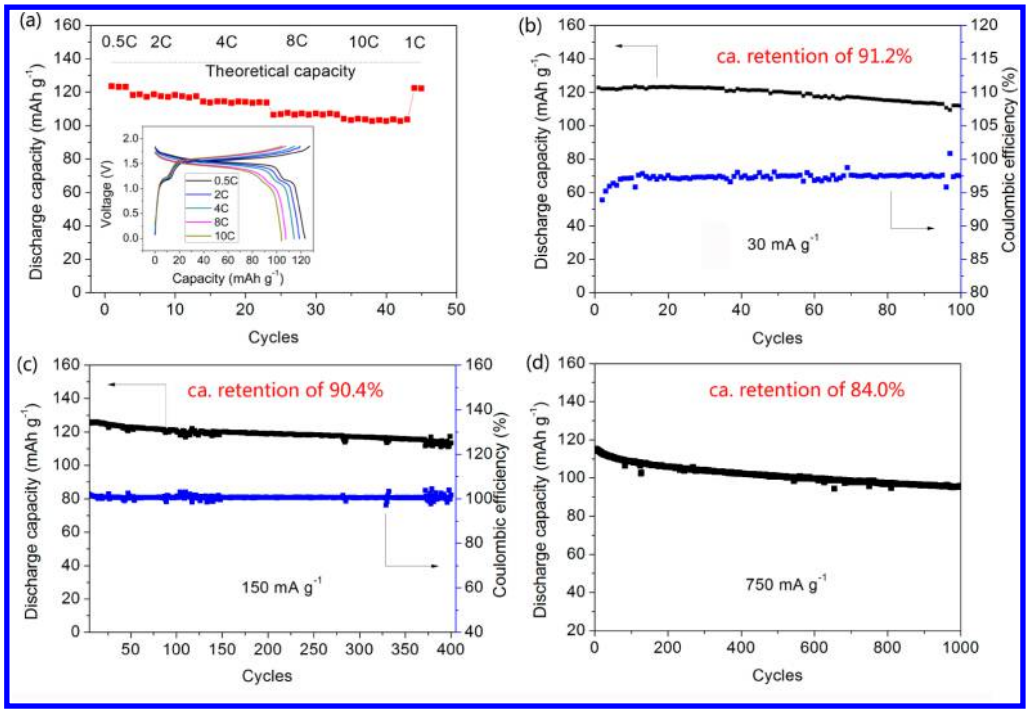

Figure 7. (a) Rate performance of LTP-T-U//$LiMn_2O_4$ ALIB and (inset) corresponding charge/discharge curves at different rates; cycling stability and Coulombic efficiency of LTP-T-U//$LiMn_2O_4$ ALIB at (b) 0.2C and (c) 1C; and (d) cycling stability of LTP-T-U//$LiMn_2O_4$ ALIB at 5C.

$LiMn_2O_4$. Excellent kinetics behaviors demonstrate the promising employment of LTP-T-U and LMO as anode and cathode for ALIB, respectively. The full cell rate performance of LTP-T-U//$LiMn_2O_4$ is shown in Figure 7a. As seen, the LTP-T-U demonstrates superior rate capability with a discharge capacity of 123 mAh g^{-1} at 150 mA g^{-1} (based on the mass of $LiTi_2(PO_4)_3$) and 103 mAh g^{-1} at 1500 mA g^{-1}. Figure 7a (inset) gives the corresponding charge/discharge curves of LTP-T-U//$LiMn_2O_4$ ALIB at different rates. A long voltage plateau around 1.55 V and a short plateau around 1.0 V are observed at low current densities. Although the discharge voltage decreases slightly on increasing current density, the potential plateau at a high rate of 10C remains well. We did not evaluate much higher rate properties of LTP-T-U as an anode in ALIBs since it is depended on both cathode and anode materials. Note that the rate capability of the used commercial $LiMn_2O_4$ (Figure S4) is not so good as LTP-T-U (Table S4). So the rate capability of the full cell would be limited by the cathode in this situation.

Long-term cycling performance of ALIB at various rates was performed. As shown in Figure 7(b–d), the ALIB demonstrates outstanding cycling stability at different rates. At a low rate of 0.2C, it delivers a discharge capacity of 123 mAh g^{-1}, and capacity retention of 91.2% after 100 cycles (Figure 6b). As the rate increases to 1C, capacity retention of 90.4% after 400 cycles is demonstrated (Figure 6c). At 5C, LTP-T-U still gives a capacity retention rate of 84.0% even after 1000 cycles (Figure 7d). These results clearly demonstrate that LTL-T-U can be tolerant to various charge/discharge rates. As we know, the poor cycling stability at low current densities is still a critical challenge for ALIBs. The crystal deterioration of electrode, reaction between electrode materials and water or O_2, and decomposition of water are considered the main causes for the capacity fading.[5,7] The cycling performance of ALIB here at low rate (e.g., 0.2C) is much superior to most of the reported ALIBs using vanadium oxides, vanadates or $LiTi_2(PO_4)_3$/C to date (Table S5).[5,7,9,11] Note that $LiTi_2(PO_4)_3$/C with capacity retention of 90% after 300 cycles was also reported by our group.[17] Low Coulombic efficiency owing to the reactions between electrode surface and aqueous electrolyte and the decomposition of water, is considered as a significant cause of capacity fading for ALIB.[5,7] As demonstrated, the ALIB here delivers high average Coulombic efficiency at various current densities (>95% at 0.2C and >99% at 1C in Figure 7b,c), in good accordance with the superior cycling performance. The excellent electrochemical properties of LTP-T-U in ALIB indicate that this nitrogen-rich carbon coated $LiTi_2(PO_4)_3$ composite with unique mesoporous structure could be used as a promising anode for high-power ALIB.

According to the above discussion, the excellent electrochemical properties of LTP-T-U are ascribed to the following factors: (1) The unique mesoporous structure. This structure has been confirmed to be superior to the common ones (e.g., bulk, nanoparticles)[28,52,53] with the advantages of larger BET surface, and more abundant nanopores could enlarge the electrolyte/electrode interfacial area, shorten Li^+ diffusion distance, relieve the mechanical lattice strain upon Li^+ insertion/extraction, and so on.[54] (2) Homogeneous nitrogen-rich carbon coating. It is well accepted that the electrochemical performance of electrode greatly depends on the state of surface carbon layer (e.g., thickness, uniformity, composition, degree of ordering, electron cloud distribution, etc.).[19,20] Undoubtedly, the well-distributed carbon layer with suitable thickness and the high-content pyridinic- and pyrrolic-type nitrogen in carbon layer could contribute significantly to the electrochemical properties. It has been confirmed that the hybridization of lone pair electrons of N atom with the π electrons in carbon will facilitate the electron diffusion, leading to higher electronic conductivity.[40]

DOI: 10.1021/acsami.5b08697
ACS Appl. Mater. Interfaces 2015, 7, 28337−28345

CONCLUSIONS

In summary, a bi-nitrogen sources doping method was proposed for the first time to achieve mesoporous $LiTi_2(PO_4)_3$@N-rich doped carbon composite. In organic LIBs, the electrode delivered ultrahigh rate performance with a discharge capacity of 101 mAh g^{-1} at 40C and 87 mAh g^{-1} at 50C. When used as an anode for ALIB, striking long cycling stability with capacity retention of 91.2% at a low current density of 0.2C after 100 cycles and 90.4% at 1C after 400 cycles was demonstrated. Superior rate capability with discharge capacity of 123 mAh g^{-1} at 1C and 103 mAh g^{-1} at 10C were also presented. The homogeneous nitrogen-rich carbon coating and the unique mesoporous structure have been verified as important factors. By virtue of its superior electrochemical performance, this composite prepared in the present study could meet the requirement of fast charge/discharge for LIBs and ALIBs. This bi-nitrogen source doping strategy may provide a reference for the fabrication of other electrode materials with nitrogen-rich carbon coating, including $Li_4Ti_5O_{12}$/C, $LiV_2(PO_4)_3$/C, $LiFePO_4$/C, and so on.

METHODS

Synthesis of LTP-T-U and LTP-T Composite. First, 0.887 g of phosphoric acid (H_3PO_4) and 0.1 g of $CO(NH_2)_2$ were dissolved in ethanol. Then, 0.2 g of $C_3H_6N_6$ was dissolved in glycol with a heating temperature of 60 °C. Next, 1.74 g of tetrabutyl titanate and 0.261 g of lithium acetate were dissolved in ethanol with stirring. Then, (H_3PO_4+$CO(NH_2)_2$)/ethanol solution and $C_3H_6N_6$/glycol solution were added dropwise into the mixed solution orderly. Afterward, the mixed solution was refluxed at 80 °C for 5 h. Then, the refluxed system was removed, and the temperature was raised to 80 °C to evaporate the solvent. After being ground by agate mortar, the resulting precursor was sintered in a tube furnace with a calcination temperature of 700 °C for 6 h under Ar gas. The as-prepared sample was named LTP-T-U.

For comparison, the sample was also fabricated by a similar process except for the addition of $CO(NH_2)_2$ (named as LTP-T).

Characterizations. X-ray diffraction data were obtained by X-ray diffractometer using Cu Kα1 radiation (Dandong Haoyuan, DX-2700). Transmission electron microscope (TEM), high-resolution TEM (HRTEM) pictures, and STEM-EDS elemental mapping of as-prepared $LiTi_2(PO_4)_3$/C powder were obtained using a FEI Tecnai G2 F20 S-TWIX TEM. Scanning electron microscope (SEM) pictures were conducted on a Nova NanoSEM 230 SEM. LabRAM Aramis (HORIBA Jobin Yvon) spectrometer was employed to record Raman spectra. Thermogravimetric analysis (TGA) was carried out on a STA 449C from 25 to 800 °C with a heating rate of 10 °C/min. The four-point probe method was used to measure the electronic conductivity (Guangzhou 4 Probes Tech, RTS-9). The XPS fitting was performed using XPSPEAK software.

Electrochemical Measurements. The electrochemical tests were all performed in a CR2016-type coin cell. For the fabrication of electrode, the active material, Polytetrafluoroethylene (PTFE), and Super P carbon in a weight ratio of 8:1:1 was mixed first, and distilled water was used as solvent. Then, the mixture was pressed on a stainless steel mesh collector under 20 MPa. After drying at 110 °C under vacuum overnight, the electrodes, whose mass loading of the active material is about 6 mg cm^{-2}, were assembled into CR2016 coin-type cells in an Ar-filled Mikrouna glovebox using Li metal as counter electrode. The electrolyte was 1 M $LiPF_6$ in 1:1 v/v ethylene carbonate/dimethyl carbonate (Guangzhou Tinci Materials Technology Co., Ltd.). The cells are cycled galvanostatically between 1.5 and 3.5 V (vs Li^+ /Li) using a Neware battery testing system (CT-3008W) at a constant temperature of 30 °C. Cyclic voltammetry (CV) curves were performed by CHI 660d electrochemical station (Shanghai Chenhua, China). Electrochemical impedance spectroscopy (EIS) was tested in a Princeton workstation (PARSTAT2273, EG&G, Salem, MA) over the frequency range from 100 kHz to 10 mHz with an amplitude of 5 mV. Before EIS test, the cells were charged to 2.5 V and then kept at that voltage via a constant voltage mode.

The electrochemical properties in aqueous electrolyte was also performed in a CR2016-type coin, which is composed of commercial $LiMn_2O_4$ as cathode, 2 mol L^{-1} Li_2SO_4 solution as electrolyte and as-prepared $LiTi_2(PO_4)_3$/C as anode. The $LiMn_2O_4$ electrodes, which were purchased from Hunan Reshine New Material Co., Ltd., were made in a similar way as $LiTi_2(PO_4)_3$/C. An excessive $LiMn_2O_4$, with cathode/anode mass ratio of (1.5−2.0)/1 was designed to better evaluate the electrochemical properties of $LiTi_2(PO_4)_3$. To eliminate the soluble oxygen, the Li_2SO_4 electrolyte was pretreated by flowing argon injection into the solution. Charge/discharge tests were performed under a designed current density by a Neware battery testing system (CT-3008W) between 0 and 1.85 V at a constant temperature of 30 °C. The capacity was measured based on the weight of the $LiTi_2(PO_4)_3$.

ASSOCIATED CONTENT

Supporting Information

The Supporting Information is available free of charge on the ACS Publications website at DOI: 10.1021/acsami.5b08697.

Lattice parameters, N_2 adsorption−desorption isotherm, high-resolution XPS images, I_{pa}/I_{pc} value, and impedance values of LTP-T and LTP-T-U. Rate capability of commercial $LiMn_2O_4$. (PDF)

AUTHOR INFORMATION

Corresponding Authors

*E-mail: wanghy419@126.com.
*E-mail: gzcao@u.washington.edu.

Notes

The authors declare no competing financial interest.

ACKNOWLEDGMENTS

This work was supported by the National Nature Science Foundation of China (No.21301193), the China Postdoctoral Science Foundation Funded Project (No.2014T70781), the Hunan Provincial Natural Science Foundation of China (No.14JJ3022), the Fundamental Research Funds for the Central Universities of Central South University, and the Opening Project of State Key Laboratory of Powder Metallurgy.

REFERENCES

(1) Armand, M.; Tarascon, J. M. Building Better Batteries. *Nature* **2008**, *451*, 652−657.

(2) Kim, H.; Hong, J.; Park, K. Y.; Kim, H.; Kim, S. W.; Kang, K. Aqueous Rechargeable Li and Na Ion Batteries. *Chem. Rev.* **2014**, *114*, 11788−11827.

(3) He, P.; Liu, J.-L.; Cui, W.-J.; Luo, J.-Y.; Xia, Y.-Y. Investigation on Capacity Fading of $LiFePO_4$ in Aqueous Electrolyte. *Electrochim. Acta* **2011**, *56*, 2351−2357.

(4) Wang, Y. G.; Luo, J. Y.; Wang, C. X.; Xia, Y. Y. Hybrid Aqueous Energy Storage Cells Using Activated Carbon and Lithium-Ion Intercalated Compounds II. Comparison of Li Mn_2O_4, Li $Co_{1/3}Ni_{1/3}Mn_{1/3}O_2$, and $LiCoO_2$ Positive Electrodes. *J. Electrochem. Soc.* **2006**, *153*, A1425−A1431.

(5) Tang, W.; Zhu, Y.; Hou, Y.; Liu, L.; Wu, Y.; Loh, K. P.; Zhang, H.; Zhu, K. Aqueous Rechargeable Lithium Batteries as an Energy Storage System of Superfast Charging. *Energy Environ. Sci.* **2013**, *6*, 2093−2104.

(6) Cui, Y.; Yuan, Z.; Bao, W.; Zhuang, Q.; Sun, Z. Investigation of Lithium Ion Kinetics through $LiMn_2O_4$ Electrode in Aqueous Li_2SO_4 Electrolyte. *J. Appl. Electrochem.* **2012**, *42*, 883−891.

DOI: 10.1021/acsami.5b08697
ACS Appl. Mater. Interfaces 2015, 7, 28337−28345

(7) Wang, Y.; Yi, J.; Xia, Y. Recent Progress in Aqueous Lithium-ion Batteries. *Adv. Energy Mater.* **2012**, *2*, 830−840.
(8) Li, W.; Dahn, J. R.; Wainwright, D. S. Rechargeable Lithium Batteries with Aqueous Electrolytes. *Science* **1994**, *264*, 1115−1118.
(9) Sun, D.; Jin, G.; Wang, H.; Liu, P.; Ren, Y.; Jiang, Y.; Tang, Y.; Huang, X. Aqueous Rechargeable Lithium Batteries using NaV_6O_{15} Nanoflakes as High Performance Anodes. *J. Mater. Chem. A* **2014**, *2*, 12999−13005.
(10) Wang, H.; Tang, Y.; Zhou, D.; Liu, S.; Zhang, H. MV_3O_8 (M = Li^+, Na^+, NH_4^+) as Novel Intercalated Materials for Li-Ion Batteries. *Prog. Chem.* **2013**, *25*, 927−939.
(11) Zhou, D.; Liu, S.; Wang, H.; Yan, G. $Na_2V_6O_{16}{\cdot}0.14H_2O$ Nanowires as a Novel Anode Material for Aqueous Rechargeable Lithium Battery with Good Cycling Performance. *J. Power Sources* **2013**, *227*, 111−117.
(12) Luo, J. Y.; Cui, W. J.; He, P.; Xia, Y.-Y. Raising the Cycling Stability of Aqueous Lithium-Ion Batteries by Eliminating Oxygen in the Electrolyte. *Nat. Chem.* **2010**, *2*, 760−765.
(13) Nuspl, G.; Takeuchi, T.; Weiß, A.; Kageyama, H.; Yoshizawa, K.; Yamabe, T. Lithium Ion Migration Pathways in $LiTi_2(PO_4)_3$ and Related Materials. *J. Appl. Phys.* **1999**, *86*, 5484−5491.
(14) Shen, L.; Zhang, X.; Uchaker, E.; Yuan, C.; Cao, G. $Li_4Ti_5O_{12}$ Nanoparticles Embedded in a Mesoporous Carbon Matrix as a Superior Anode Material for High Rate Lithium Ion Batteries. *Adv. Energy Mater.* **2012**, *2*, 691−698.
(15) Wang, J.; Sun, X. Understanding and Recent Development of Carbon Coating on $LiFePO_4$ Cathode Materials for Lithium-ion Batteries. *Energy Environ. Sci.* **2012**, *5*, 5163−5185.
(16) Zhou, X.; Yin, Y. X.; Cao, A. M.; Wan, L. J.; Guo, Y. G. Efficient 3D Conducting Networks Built by Graphene Sheets and Carbon Nanoparticles for High-Performance Silicon Anode. *ACS Appl. Mater. Interfaces* **2012**, *4*, 2824−2828.
(17) Sun, D.; Jiang, Y.; Wang, H.; Yao, Y.; Xu, G.; He, K.; Liu, S.; Tang, Y.; Liu, Y.; Huang, X. Advanced Aqueous Rechargeable Lithium Battery Using Nanoparticulate $LiTi_2(PO_4)_3$/C as a Superior Anode. *Sci. Rep.* **2015**, *5*, 10733.
(18) Ai, W.; Luo, Z.; Jiang, J.; Zhu, J.; Du, Z.; Fan, Z.; Xie, L.; Zhang, H.; Huang, W.; Yu, T. Nitrogen and Sulfur Codoped Graphene: Multifunctional Electrode Materials for High-Performance Li-Ion Batteries and Oxygen Reduction Reaction. *Adv. Mater.* **2014**, *26*, 6186−6192.
(19) Wang, X.; Weng, Q.; Liu, X.; Wang, X.; Tang, D. M.; Tian, W.; Zhang, C.; Yi, W.; Liu, D.; Bando, Y.; Golberg, D. Atomistic origins of High Rate Capability and Capacity of N-doped Graphene for Lithium Storage. *Nano Lett.* **2014**, *14*, 1164−1171.
(20) Qiu, Y.; Li, W.; Zhao, W.; Li, G.; Hou, Y.; Liu, M.; Zhou, L.; Ye, F.; Li, H.; Wei, Z.; et al. High-Rate, Ultralong Cycle-Life Lithium/Sulfur Batteries Enabled by Nitrogen-Doped Graphene. *Nano Lett.* **2014**, *14*, 4821−4827.
(21) Hou, Y.; Li, J.; Wen, Z.; Cui, S.; Yuan, C.; Chen, J. N-doped Graphene/Porous g-C3N4 Nanosheets Supported Layered-MoS_2 Hybrid as Robust Anode Materials for Lithium-ion Batteries. *Nano Energy* **2014**, *8*, 157−164.
(22) Zhou, X.; Wan, L.-J.; Guo, Y.-G. Binding SnO_2 Nanocrystals in Nitrogen-Doped Graphene Sheets as Anode Materials for Lithium-Ion Batteries. *Adv. Mater.* **2013**, *25*, 2152−2157.
(23) Luo, W.; Wang, B.; Heron, C. G.; Allen, M. J.; Morre, J.; Maier, C. S.; Stickle, W. F.; Ji, X. Pyrolysis of Cellulose under Ammonia Leads to Nitrogen-Doped Nanoporous Carbon Generated through Methane Formation. *Nano Lett.* **2014**, *14*, 2225−2229.
(24) Zhu, Z.; Wang, S.; Du, J.; Jin, Q.; Zhang, T.; Cheng, F.; Chen, J. Ultrasmall Sn Nanoparticles Embedded in Nitrogen-doped Porous Carbon as Hgh-performance Anode for Lithium-Ion Batteries. *Nano Lett.* **2014**, *14*, 153−157.
(25) Zhou, X.; Bao, J.; Dai, Z.; Guo, Y.-G. Tin Nanoparticles Impregnated in Nitrogen-Doped Graphene for Lithium-Ion Battery Anodes. *J. Phys. Chem. C* **2013**, *117*, 25367−25373.
(26) Yang, J.; Wang, J.; Li, X.; Wang, D.; Liu, J.; Liang, G.; Gauthier, M.; Li, Y.; Geng, D.; Li, R.; Sun, X. Hierarchically Porous $LiFePO_4$/Nitrogen-Doped Carbon Nanotubes Composite as a Cathode for Lithium Ion Batteries. *J. Mater. Chem.* **2012**, *22*, 7537−7543.
(27) Lei, C.; Han, F.; Li, D.; Li, W.-C.; Sun, Q.; Zhang, X.-Q.; Lu, A.-H. Dopamine as the Coating Agent and Carbon Precursor for the Fabrication of N-doped Carbon Coated Fe_3O_4 Composites as Superior Lithium Ion Anodes. *Nanoscale* **2013**, *5*, 1168−1175.
(28) Ren, Y.; Ma, Z.; Bruce, P. G. Ordered Mesoporous Metal oxides: Synthesis and Applications. *Chem. Soc. Rev.* **2012**, *41*, 4909−4927.
(29) Wang, G.; Liu, H.; Liu, J.; Qiao, S.; Lu, G. M.; Munroe, P.; Ahn, H. Mesoporous $LiFePO_4$/C Nanocomposite Cathode Materials for High Power Lithium Ion Batteries with Superior Performance. *Adv. Mater.* **2010**, *22*, 4944−4948.
(30) Wei, Q.; An, Q.; Chen, D.; Mai, L.; Chen, S.; Zhao, Y.; Hercule, K. M.; Xu, L.; Minhas-Khan, A.; Zhang, Q. One-Pot Synthesized Bicontinuous Hierarchical $Li_3V_2(PO_4)_3$/C Mesoporous Nanowires for High-Rate and Ultralong-Life Lithium-Ion Batteries. *Nano Lett.* **2014**, *14*, 1042−1048.
(31) Bruce, P. G.; Scrosati, B.; Tarascon, J.-M. Nanomaterials for Rechargeable Lithium Batteries. *Angew. Chem., Int. Ed.* **2008**, *47*, 2930−2946.
(32) Wu, Z.-S.; Ren, W.; Xu, L.; Li, F.; Cheng, H.-M. Doped Graphene Sheets As Anode Materials with Superhigh Rate and Large Capacity for Lithium Ion Batteries. *ACS Nano* **2011**, *5*, 5463−5471.
(33) Jiao, W.; Li, N.; Wang, L.; Wen, L.; Li, F.; Liu, G.; Cheng, H.-M. High-Rate Lithium Storage of Anatase TiO_2 Crystals Doped with Both Nitrogen and Sulfur. *Chem. Commun.* **2013**, *49*, 3461−3463.
(34) Luo, J. Y.; Xia, Y. Y. Aqueous Lithium-ion Battery $LiTi_2(PO_4)_3$/$LiMn_2O_4$ with High Power and Energy Densities as well as Superior Cycling Stability. *Adv. Funct. Mater.* **2007**, *17*, 3877−3884.
(35) Shivashankaraiah, R. B.; Manjunatha, H.; Mahesh, K. C.; Suresh, G. S.; Venkatesha, T. V. Electrochemical Characterization of $LiTi_2(PO_4)_3$ as Anode Material for Aqueous Rechargeable Lithium Batteries. *J. Electrochem. Soc.* **2012**, *159*, A1074−A1082.
(36) Xiao, W.; Miao, C.; Yin, X.; Zheng, Y.; Tian, M.; Li, H.; Mei, P. Effect of Urea as Pore-forming Agent on Properties of Poly(vinylidene fluoride-co-hexafluoropropylene)-based Gel Polymer Electrolyte. *J. Power Sources* **2014**, *252*, 14−20.
(37) Yue, Y.; Binder, A. J.; Guo, B.; Zhang, Z.; Qiao, Z.-A.; Tian, C.; Dai, S. Mesoporous Prussian Blue Analogues: Template-Free Synthesis and Sodium-Ion Battery Applications. *Angew. Chem., Int. Ed.* **2014**, *53*, 3134−3137.
(38) Wei, D.; Liu, Y.; Wang, Y.; Zhang, H.; Huang, L.; Yu, G. Synthesis of N-Doped Graphene by Chemical Vapor Deposition and Its Electrical Properties. *Nano Lett.* **2009**, *9*, 1752−1758.
(39) Lu, Y. F.; Lo, S. T.; Lin, J. C.; Zhang, W.; Lu, J. Y.; Liu, F. H.; Tseng, C. M.; Lee, Y. H.; Liang, C. T.; Li, L. J. Nitrogen-Doped Graphene Sheets Grown by Chemical Vapor Deposition: Synthesis and Influence of Nitrogen Impurities on Carrier Transport. *ACS Nano* **2013**, *7*, 6522−6532.
(40) Li, Z.; Xu, Z.; Tan, X.; Wang, H.; Holt, C. M. B.; Stephenson, T.; Olsen, B. C.; Mitlin, D. Mesoporous Nitrogen-Rich Carbons Derived From Protein for Ultra-High Capacity Battery Anodes and Supercapacitors. *Energy Environ. Sci.* **2013**, *6*, 871−878.
(41) Luo, J. Y.; Chen, L. J.; Zhao, Y. J.; He, P.; Xia, Y. Y. The Effect of Oxygen Vacancies on the Structure and Electrochemistry of $LiTi_2(PO_4)_3$ for Lithium-Ion Batteries: A Combined Experimental and Theoretical Study. *J. Power Sources* **2009**, *194*, 1075−1080.
(42) Zhao, L.; Hu, Y. S.; Li, H.; Wang, Z.; Chen, L. Porous $Li_4Ti_5O_{12}$ Coated with N-Doped Carbon from Ionic Liquids for Li-Ion Batteries. *Adv. Mater.* **2011**, *23*, 1385−1388.
(43) Ma, C.; Shao, X.; Cao, D. Nitrogen-Doped Graphene Nanosheets as Anode Materials for Lithium Ion Batteries: A First-Principles Study. *J. Mater. Chem.* **2012**, *22*, 8911−8915.
(44) Yuan, L. X.; Wang, Z. H.; Zhang, W. X.; Hu, X. L.; Chen, J. T.; Huang, Y. H.; Goodenough, J. B. Development and Challenges of $LiFePO_4$ Cathode Material for Lithium-Ion Batteries. *Energy Environ. Sci.* **2011**, *4*, 269−284.

DOI: 10.1021/acsami.5b08697
ACS Appl. Mater. Interfaces 2015, 7, 28337−28345

(45) Zhou, X.; Wang, F.; Zhu, Y.; Liu, Z. Graphene Modified $LiFePO_4$ Cathode Materials for High Power Lithium Ion Batteries. *J. Mater. Chem.* **2011**, *21*, 3353−3358.
(46) Wan, Z.; Cai, R.; Jiang, S.; Shao, Z. Nitrogen-and TiN-modified $Li_4Ti_5O_{12}$: One-Step Synthesis and Electrochemical Performance Optimization. *J. Mater. Chem.* **2012**, *22*, 17773−17781.
(47) Cheng, F.; Wang, H.; Zhu, Z.; Wang, Y.; Zhang, T.; Tao, Z.; Chen, J. Porous $LiMn_2O_4$ Nanorods with Durable High-Rate Capability for Rechargeable Li-Ion Batteries. *Energy Environ. Sci.* **2011**, *4*, 3668−3675.
(48) Wang, H.; Liu, S.; Ren, Y.; Wang, W.; Tang, A. Ultrathin $Na_{1.08}V_3O_8$ Nanosheets-a Novel Cathode Material with Superior Rate Capability and Cycling Stability for Li-Ion Batteries. *Energy Environ. Sci.* **2012**, *5*, 6173−6179.
(49) Zhu, Y.; Wang, C. Novel CV for Phase Transformation Electrodes. *J. Phys. Chem. C* **2011**, *115*, 823−832.
(50) Sun, D.; Jin, G.; Wang, H.; Huang, X.; Ren, Y.; Jiang, J.; He, H.; Tang, Y. $Li_xV_2O_5/LiV_3O_8$ Nanoflakes with Significantly Improved Electrochemical Performance for Li-Ion Batteries. *J. Mater. Chem. A* **2014**, *2*, 8009−8016.
(51) Wang, H.; Huang, K.; Ren, Y.; Huang, X.; Liu, S.; Wang, W. $NH_4V_3O_8$/carbon Nanotubes Composite Cathode Material with High Capacity and Good Rate Capability. *J. Power Sources* **2011**, *196*, 9786−9791.
(52) Jiao, F.; Bao, J.; Bruce, P. G. Factors Influencing the Rate of Fe_2O_3 Conversion Reaction. *Electrochem. Solid-State Lett.* **2007**, *10*, A264−A266.
(53) Ren, Y.; Armstrong, A. R.; Jiao, F.; Bruce, P. G. Influence of Size on the Rate of Mesoporous Electrodes for Lithium Batteries. *J. Am. Chem. Soc.* **2010**, *132*, 996−1004.
(54) Qu, Q.; Fu, L.; Zhan, X.; Samuelis, D.; Maier, J.; Li, L.; Tian, S.; Li, Z.; Wu, Y. Porous $LiMn_2O_4$ as Cathode Material with High Power and Excellent Cycling for Aqueous Rechargeable Lithium Batteries. *Energy Environ. Sci.* **2011**, *4*, 3985−3990.

DOI: 10.1021/acsami.5b08697
ACS Appl. Mater. Interfaces 2015, 7, 28337−28345